PERGAMON

International Journal of Multiphase Flow 25 (1999) 155–173

International Journal of Multiphase Flow

Sensitivity study on double-sensor conductivity probe for the measurement of interfacial area concentration in bubbly flow

Q. Wu [a,*], M. Ishii [b]

[a] *Department of Nuclear Engineering, Oregon State University, Corvallis, OR 97331, USA*
[b] *Thermal Hydraulics and Reactor Safety Laboratory, School of Nuclear Engineering, Purdue University, West Lafayette, IN 47907, USA*

Received 1 May 1997; received in revised form 13 March 1998

Abstract

The sensitivity study on a double-sensor conductivity probe for the measurement of local interfacial area concentration, has been carried out by considering the effects of bubble lateral motions and probe spacing. The measurable value was rigorously related to the local bubble interface velocity in the surface normal direction, and the probability density function of each individual variable was identified with proper coordinate transform. Three theoretical calibration factors were defined to bridge the mean measurable parameter to the interfacial area concentrations carried by the missed bubbles, measured bubbles and their combination. These calibration factors were obtained through numerical method. The results indicate that the total calibration factor is the best choice for practical applications, whereas the other two factors bring in profound understandings of the measuring mechanisms. With the probe spacing varying from about 36–86% of the mean bubble diameter, the total calibration factor is only determined by the bubble velocity fluctuation, almost independent of the probe spacing. The analysis also suggests that the missed bubbles contribute larger interfacial area concentration to the measuring point than that obtained from the measured bubbles. Moreover, for better statistic behaviors, the appropriate sample size was provided using a Monte Carlo approach.

Keywords: Interfacial area; Two-phase flow measurement; Conductivity probe; Bubble velocity

* Corresponding author.

PII: S0301-9322(98)00037-8

1. Introduction

Interfacial area concentration in two-phase flow is defined as the total interface area per unit mixture volume. In the two-fluid model (Vernier and Delhaye, 1968; Ishii, 1975; Boure, 1978), this parameter specifies the geometric capability of the interfacial mass, momentum and energy transfers, because these interfacial transfers between the two-phases are basically proportional to the available interface area. Therefore, the knowledge of interfacial area concentration is indispensable in the two-fluid model. However, most of the available experimental data are limited to volume or line averaged values over a section of a flow channel (Veteau and Charlot, 1981; Landau, 1977). Recently, double-sensor and four-sensor conductivity probes were developed to measure the local time-averaged interfacial area concentration by Kataoka et al. (1986). For the double-sensor probe, they took into account the lateral movements of the measured bubbles and obtained a theoretical calibration factor smaller than that without considering the lateral bubble velocity components (Herringe and Davis, 1976). According to Kataoka et al. (1986), the measured parameters can be transformed to the interfacial area concentration carried by the detected bubbles, whereas the interfacial area concentration carried by the missed bubbles is recovered as if they possess the measured average value. Later in 1994, they furthered the study on the effects of the probe-tip separation using a Monte Carlo approach, and concluded that the probe spacing had little effect on the proposed calibration factor, if the probe spacing was smaller than 1/5 of the measured bubble diameter (Kataoka et al., 1994).

In this study, both the bubble lateral velocity components and the probe spacing are considered to rigorously derive the theoretical calibration factor for the measurement of local interfacial area concentration, by means of the double-sensor conductivity probe technique. The basic assumptions in this study are isotropic bubble velocity fluctuations and spherical bubble shapes. The assumption of isotropic bubble velocity fluctuation is due to the consideration that the irregular bubble motion is mainly cased by turbulent eddies in the continuous medium. The motions of these eddies are approximately isotropic with a first-order accuracy. For some other practical bubble velocity distributions, however, the proposed method in this study is still valid by simply replacing the isotropic probability density distribution function. On the other hand, the hypothesis on the bubble sphericity is much more restrictive, which limits the proposed analysis for only finely dispersed bubbly flow. Further studies are needed for the measurement of non-spherical bubbles. For distorted or cap bubbles, the bubble–probe interactions as well as the unpredictable surface normal directions make the measurement virtually impossible. In such a situation, a four-sensor probe technique was proposed to depict the actual velocity direction of an interface (Leung, 1996). However, because of the large physical size of the four-sensor probe, this method in its present stage is not applicable for small bubbles.

With these assumptions, the influences of the bubble lateral motion and the finite probe spacing on the measurement are examined in Section 2, and the mechanisms responsible for the missing bubble phenomena in the measurement are clearly identified. Thereafter, three theoretical calibration factors are proposed to bridge the mean measurable parameter to the local interfacial area concentrations carried by the measured bubbles, the missed bubbles and their combination. To obtain these calibration factors, certain averaging operations are

performed with the probability density function of each individual variable obtained from appropriate coordinate transformation. Owing to the difficulty in analytical solutions, numerical approach is employed to study the theoretical calibration factors with respect to the variations of the bubble velocity fluctuation and the probe spacing. In Section 3, detailed analyses of the numerical results indicate that the total calibration factor is the best choice for practical applications. This factor is a function of the bubble velocity fluctuation, almost independent of the probe spacing, if the bubble diameter varies from 1.2 to 2.8 times the probe spacing. Different from the result of Kataoka et al. (1986), this factor is larger than that without considering the lateral components of the bubble velocity fluctuation. The analysis also suggests that the missed bubbles carry larger interfacial area concentration than that carried by the measured bubbles. Hence, the conventional method for the recovery of the missed bubbles may cause significant uncertainty. In Section 3, a method is also provided to determine the relative bubble velocity fluctuation in terms of the measured values from a finite sample base. Moreover, for reasonable statistic behavior, the necessary sample size is evaluated using a Monte Carlo approach.

2. Principle of measurement and theoretical calibration

According to Ishii (1975), the definition of the local interfacial area concentration is given by:

$$\bar{a}^{\,t} = \frac{1}{\Delta T}\sum_j \left(\frac{1}{|\mathbf{V}_i \cdot \mathbf{n}_i|}\right)_j, \tag{1}$$

where the index j denotes the jth interface that passes the point of interest during a time interval, ΔT, of time averaging. $\mathbf{V}_i$ and $\mathbf{n}_i$ refer to the local bubble interface velocity and surface normal vector, respectively. For a local measurement technique, it is thus necessary to quantify the interface velocity in the surface normal direction, either directly or indirectly.

The double-sensor conductivity probe made at Purdue University is designed with two thin electrodes, as shown schematically in Fig. 1. The tip of each electrode exposes a two-phase mixture, and measures the impedance between the probe tip and the common ground. Owing to the large difference in conductivity between liquid phase and the gas bubbles, the impedance signal rises sharply when a bubble passes through the probe. As the diameter of the probe tips is very small (89 μm in diameter), no significant bubble deformation or fragmentation is observed through flow visualization for the studied bubble size range between 2 and 4 mm (Leung 1996), and thus the time delay, Δt, of the two impedance signals, can be utilized to characterize the time-interval for the bubble surface traveling from the front probe tip to the back tip. With a known separation of the two probe tips, defined as Δs, a measurable bubble "velocity", $V_m = \Delta s/\Delta t$, is obtained. In a real two-phase bubbly flow, bubbles have variable shapes and move in a complicated manner. It is extremely difficult to find the relation between this measurable value and the interface velocity in the surface normal direction. However, if

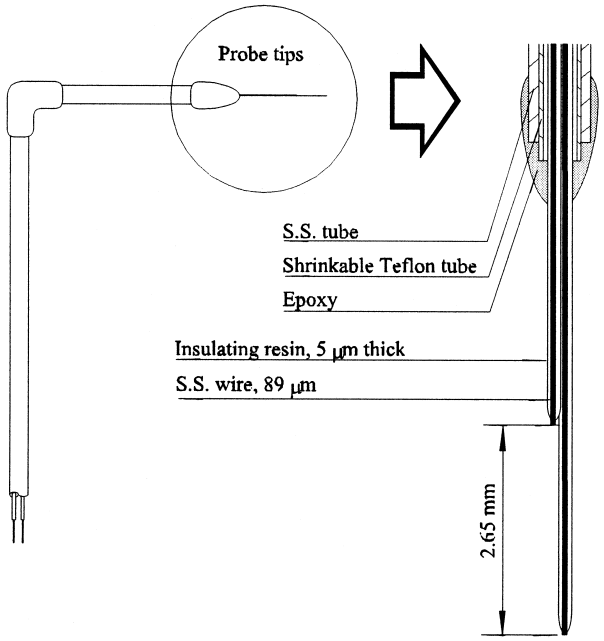

Fig. 1. Schematic diagram of double-sensor conductivity probe.

the bubbles have spherical shapes without size changes and do not alter their moving courses between the two probe tips, the measurable value can be transformed to the average interface velocity in the surface normal direction through certain statistic analyses. The hypothesis on the bubble sphericity limits the technique for the applications to finely dispersed bubbly flow. For the measurement distorted or cap bubbles, the bubble–probe interactions, as well as the unpredictable surface normal directions, make the measurement virtually impossible. In such a situation, a four-sensor probe technique was proposed to depict the actual velocity direction of an interface (Kataoka et al. 1986). However, because of the large physical size of the four-sensor probe, this method in the present stage is not applicable for small bubbles.

First, let us consider a very simple case when the bubbles move in the direction parallel to the probe orientation, and then identify the important parameters that need to be involved in practical measurement. Under the restriction of unidirectional bubble movements, the measurable value, $\Delta s/\Delta t$, is identical to the magnitude of the bubble velocity. From the definition of [1], the local interfacial area concentration is given by:

$$\bar{a}^{\mathrm{t}} = \frac{1}{\Delta T}\sum_j \left(\frac{1}{|\mathbf{V}_i \cdot \mathbf{n}_i|}\right)_j = \frac{1}{\Delta T}\sum_j \left(\frac{\Delta t}{\Delta s \cos\theta}\right)_j, \tag{2}$$

where θ is the angle between the surface normal vector and the bubble velocity (in the z-direction). Since there is no correlation between the velocity magnitude and the angle, if the sample size is sufficiently large, the summation can be approximated by an integral weighted by

a probability distribution function, $P(\theta)$, in the following form:

$$\bar{a}^{\mathrm{t}} = \frac{2}{\Delta T}\sum_j \left(\frac{\Delta t}{\Delta s}\right)_j \int_0^{\pi/2} \frac{P(\theta)}{\cos\theta}\,\mathrm{d}\theta = \frac{2N_{\mathrm{b}}}{\Delta T}\overline{\left(\frac{\Delta t}{\Delta s}\right)} \int_0^{\pi/2} \frac{P(\theta)}{\cos\theta}\,\mathrm{d}\theta, \tag{3}$$

where, N_{b} is the number of measured bubbles, and the factor 2 is due to the two surfaces of each spherical bubble that passes through the measuring point. The bar over the term, $\Delta t/\Delta s$, means averaging of all the measured bubbles. For an equal probability distribution of the measuring points over the z-directional projected bubble area, the probability density function of θ is given by:

$$P(\theta) = 2\sin\theta\cos\theta, \quad 0 \le \theta \le \pi/2, \tag{4}$$

and (3) is then deduced to:

$$a^{\mathrm{t}} = \frac{2N_{\mathrm{b}}}{\Delta T}\overline{\left(\frac{\Delta t}{\Delta s}\right)} \int_0^{\pi/2} 2\sin\theta\,\mathrm{d}\theta = \frac{4N_b}{\Delta T}\overline{\left(\frac{\Delta t}{\Delta s}\right)}. \tag{5}$$

The integration equals 2, a calibration factor that relates the average $\Delta t/\Delta s$ to the true interfacial area concentration. This formula was widely utilized to obtain the local interfacial area concentration when the bubble velocity fluctuation is negligible.

Once the bubble velocity fluctuation is considered, however, the lateral motions of a bubble may cause complications in the measurement as shown in Fig. 2. Equation (5) then losses its theoretical base and becomes questionable. In a normal situation defined in Fig. 2(a), both probe tips penetrate in a bubble, with the impedance signal of the first probe tip ahead of the second tip. The measured ''velocity'', $V_{\mathrm{m}} = \Delta s/\Delta t$, no longer equals the true bubble velocity, and is strongly influenced by both the bubble velocity orientation and the probe spacing relative to the bubble size. Fig. 2(b) and (c) depict the missing bubble cases, where either the second probe tip cannot touch the bubble with a flat signal output, or the signal from the first tip falls behind that of the second tip. A conventional way to handle these missed bubbles is to treat them as if they possess the average measured interface velocity in the surface normal direction for the normal case, Fig. 2(a). However, from Fig. 2(b) and (c) we can tell that the missing bubble cases occur at the edge of the bubbles where the magnitude of the interface velocity in the surface normal direction, $|\mathbf{V}_i \cdot \mathbf{n}_i|$, is small. Therefore, the average interfacial area concentration of the missed bubbles at the measuring point is generally greater than that obtained in the normal situation. In view of these complications, the bubble velocity fluctuation and the probe spacing should be considered, in order to rigorously bridge the measurable value to the true local interfacial area concentration.

From the above discussion, the real local interfacial area concentration can be separated into two parts:

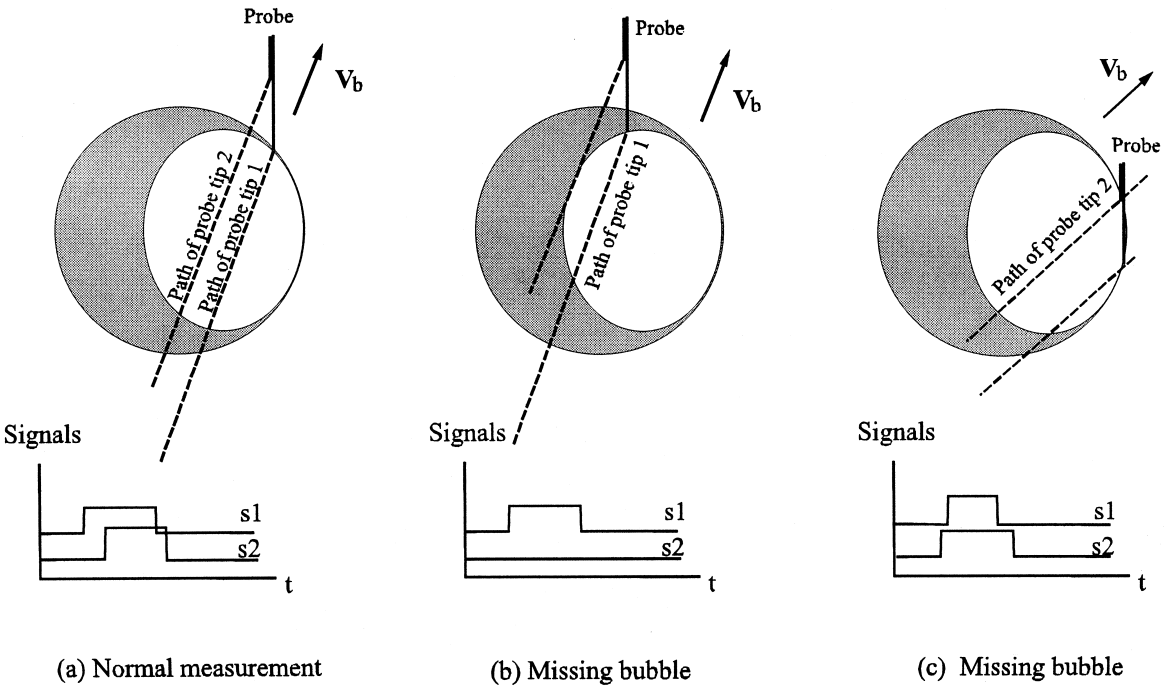

Fig. 2. Effects of bubble velocity and probe spacing on the output signals. (a) Normal measurement; (b) missing bubble; and (c) missing bubble.

$$\bar{a}_i = \frac{2N_b}{\Delta T}\overline{\left(\frac{1}{V_i(\mathbf{n}_V \cdot \mathbf{n}_i)}\right)}_{\text{total}}$$

$$= \frac{2N_b}{\Delta T}\left[\frac{N_b - N_{\text{miss}}}{N_b}\overline{\left(\frac{1}{V_i(\mathbf{n}_V \cdot \mathbf{n}_i)}\right)}_{\text{normal}} + \frac{N_{\text{miss}}}{N_b}\overline{\left(\frac{1}{V_i(\mathbf{n}_v \cdot \mathbf{n}_i)}\right)}_{\text{miss}}\right], \tag{6}$$

where $\mathbf{n}_V$ is the unit vector of the bubble velocity $\mathbf{V}_i$, and $\mathbf{n}_i$ refers to the normal vector on the bubble surface where the first probe tip hits the bubble inwardly. N_{miss} denotes the number of the missed bubbles. In the experiment, N_{miss} is readily obtained from the total number of the bubbles sensed by the first probe tip subtracting the number of the bubbles that give normal signals to the second probe tip. The sample base for the average with subscript "total", comes from all of the interfaces where the first probe tip hits the bubbles inwardly, including the normal and missing bubble cases, whereas the subscripts "normal" and "miss" refer to the normal and missing bubble cases, respectively. Meanwhile, the parameter to be acquired in experiments is the average $\Delta t/\Delta s$:

$$\overline{\left(\frac{1}{V_m}\right)}_{\text{normal}} = \frac{1}{N_b - N_{\text{miss}}}\sum_j \left(\frac{\Delta t}{\Delta s}\right)_j. \tag{7}$$

The sample base for this average comes from the normal case as demonstrated in Fig. 2(a),

excluding the missing bubble cases described in Fig. 2(b) and (c), because no time delay, Δt, for these abnormal cases can be obtained in the measurement.

In order to obtain the interfacial area concentration in terms of this measurable value, we define the following three theoretical calibration factors:

$$f_{\text{total}} = \frac{\overline{\left(\frac{1}{V_i(\mathbf{n}_V \cdot \mathbf{n}_i)}\right)}_{\text{total}}}{\overline{\left(\frac{1}{V_m}\right)}_{\text{normal}}} \tag{8}$$

$$f_{\text{normal}} = \frac{\overline{\left(\frac{1}{V_i(\mathbf{n}_V \cdot \mathbf{n}_i)}\right)}_{\text{normal}}}{\overline{\left(\frac{1}{V_m}\right)}_{\text{normal}}} \tag{9}$$

$$f_{\text{miss}} = \frac{\overline{\left(\frac{1}{V_i(\mathbf{n}_V \cdot \mathbf{n}_i)}\right)}_{\text{miss}}}{\overline{\left(\frac{1}{V_m}\right)}_{\text{normal}}}. \tag{10}$$

These factors can be obtained theoretically through statistic approach. To do so, the mathematical relation between V_i and V_m at each measuring point ought to be determined. For a spherical bubble with diameter D, (A6) in the Appendix gives the necessary relationship between the measured parameter, V_m, and the bubble velocity:

$$\frac{V_m}{V_i} = \frac{[2(\mathbf{k} \cdot \mathbf{n}_v) + \gamma(\mathbf{n}_i \cdot \mathbf{n}_V)] + \sqrt{[2(\mathbf{k} \cdot \mathbf{n}_V) + \gamma(\mathbf{n}_i \cdot \mathbf{n})_V)]^2 - 4[\gamma(\mathbf{k} \cdot \mathbf{n}_i) + 1]}}{2[\gamma(\mathbf{k} \cdot \mathbf{n}_i) + 1]} \tag{11}$$

where γ is defined as $D/\Delta s$, and $\mathbf{k}$ is the unit vector in the z-direction parallel to the probe orientation. The harmonic mean of the measured velocity is thus given by:

$$\overline{\left(\frac{1}{V_m}\right)}_{\text{normal}} = \overline{\left(\frac{2[\gamma(\mathbf{k} \cdot \mathbf{n}_i) + 1]}{V_i\left\{[2(\mathbf{k} \cdot \mathbf{n}_V) + \gamma(\mathbf{n}_i \cdot \mathbf{n}_V)] + \sqrt{[2(\mathbf{k} \cdot \mathbf{n}_V) + \gamma)\mathbf{n}_i \cdot \mathbf{n}_i \cdot \mathbf{n}_V)]^2 - 4[\gamma(\mathbf{k} \cdot \mathbf{n}_i) + 1]}\right\}}\right)}_{\text{normal}}. \tag{12}$$

For a sufficiently large sample base, this mean operation can be replaced by an integration with appropriate probability density functions for the bubble velocity and the measuring locations. Statistically, the bubble velocity, $\mathbf{V}_i$, fluctuates around a mean velocity, $\bar{V}_b$, that

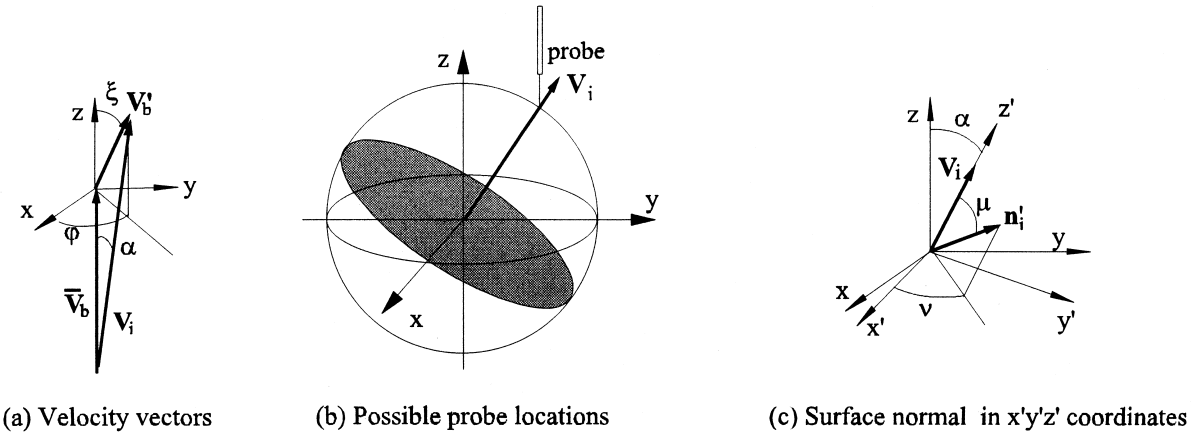

Fig. 3. Definitions of vectors and coordinate systems. (a) Velocity vectors; (b) possible probe locations; and (c) surface normal in $x'y'z'$ coordinates.

points to the z-direction, Fig. 3(a):

$$\mathbf{V}_i = \bar{V}_\mathrm{b}\mathbf{k} + \mathbf{V}'_\mathrm{b} = \bar{V}_\mathrm{b}(\mathbf{k} + H\mathbf{n}'_\mathrm{V}), \tag{13}$$

with

$$\mathbf{n}'_\mathrm{V} = \sin\xi\cos\varphi\mathbf{i} + \sin\xi\sin\varphi\mathbf{j} + \cos\xi\mathbf{k}, \tag{14}$$

where, $\mathbf{V}'_\mathrm{b}$ stands for the bubble velocity fluctuation, $\mathbf{n}'_\mathrm{V}$ represents the unit vector in the direction of the velocity fluctuation, and H refers to $V'_\mathrm{b}/\bar{V}_b$. The polar angle ξ varies from 0 to π and the azimuthal angle φ from 0 to 2π. With the assumption of isotropic bubble velocity fluctuations, the distribution function of the angles is given by:

$$P(\xi, \varphi) = \frac{1}{4\pi}\sin\xi, \quad \xi \in [0, \pi],\ \varphi \in [0, 2\pi]. \tag{15}$$

The assumption of isotropic bubble velocity fluctuation is due to the consideration that the irregular bubble motions are mainly driven by turbulent eddies in the continuous medium. The motions of these eddies are approximately isotropic with a first-order accuracy. For some other practical bubble velocity distributions, however, the proposed method in this study is still valid, by simply replacing the distribution function in (15). This hypothesis also implies that the bubble motion does not change course between the two probe tips. It is believed that only the eddies larger than the bubble size can cause significant bubble motion. Since the probe tip separation is designed smaller than the size of the bubbles to be measured, the bubble motion can persist between the two probe tips.

For the probability density function of the surface normal vector, the derivation is not straight forward. As shown in Fig. 3(b), the measuring points are uniformly distributed in the bubble cross-sectional area perpendicular to the bubble velocity direction (the shaded area). Owing to the tilted bubble velocity vector, this cross-sectional area does not always lie in the

xy-plane as assumed by Kataoka et al. (1986), and it is thus very difficult to determine the probability density functions of the directional angles in the xyz coordinates. However, if we rotate the coordinate system to a $x'y'z'$ system with its z'-axis in the bubble velocity direction as shown in Fig. 3(c), the surface normal vector at the point, where the first probe tip hits the interface inwardly, is given by:

$$\mathbf{n}_i' = \cos\mu\mathbf{k}' + \sin\mu\cos v\mathbf{i}' + \sin\mu\sin v\mathbf{j}', \tag{16}$$

and the probability density function of the polar angle μ and the azimuthal angle v should be:

$$P(\mu, v) = \frac{1}{\pi}\sin\mu\cos\mu, \quad \mu \in [0, \pi/2], \quad v \in [0, 2\pi]. \tag{17}$$

Being transformed back to the original xyz coordinates, this surface normal vector is given by:

$$\mathbf{n}_i = \mathbf{A}\cdot\mathbf{n}_i', \tag{18}$$

with

$$\mathbf{A} = \begin{bmatrix} 1-(1+\cos\alpha)\cos^2\varphi & (1+\cos\alpha)\sin\varphi\cos\varphi & \sin\alpha\cos\varphi \\ -(1+\cos\alpha)\sin\varphi\cos\varphi & (1+\cos\alpha)\sin^2\varphi - 1 & -\sin\alpha\sin\varphi \\ \sin\alpha\cos\varphi & \sin\alpha\sin\varphi & \cos\alpha \end{bmatrix}, \tag{19}$$

where $\mathbf{A}$ is a coordinate transform matrix, and α is the polar angle of the velocity vector in the xyz coordinates, as defined in Fig. 3(a) and (c), which can be related to the relative velocity fluctuation, H, and the polar angle, ξ, of the velocity fluctuation:

$$\sin\alpha = \frac{H\sin\xi}{\sqrt{(1+H\cos\xi)^2 + (H\sin\xi)^2}}, \tag{20}$$

$$\cos\alpha = \frac{(1+H\cos\xi)}{\sqrt{(1+H\cos\xi)^2 + (H\sin\xi)^2}}, \tag{21}$$

For a fixed relative velocity fluctuation, H, the surface normal vector in the original xyz coordinate system is thus a function of ξ, φ, μ and v, whose probability density functions have been determined in (15) and (17). Subsequently, the mean operations in (8)–(10) can be performed in the following way to obtain the theoretical calibration factors.

The total harmonic mean of interfacial velocity in the surface normal direction:

$$\overline{\left(\frac{1}{V_i(\mathbf{n}_\mathrm{V}\cdot\mathbf{n}_i)}\right)}_{\mathrm{total}} = \frac{1}{\bar{V}_\mathrm{b}}\int_0^{2\pi}\int_0^{\pi}\int_0^{\frac{\pi}{2}}\int_0^{2\pi}\frac{\sin\xi\sin\mu\cos\mu}{4\pi^2[(\mathbf{k}+H\mathbf{n}_\mathrm{V}')\cdot\mathbf{A}\cdot\mathbf{n}_i']}\,\mathrm{d}v\,\mathrm{d}\mu\,\mathrm{d}\xi\,\mathrm{d}\varphi \tag{22}$$

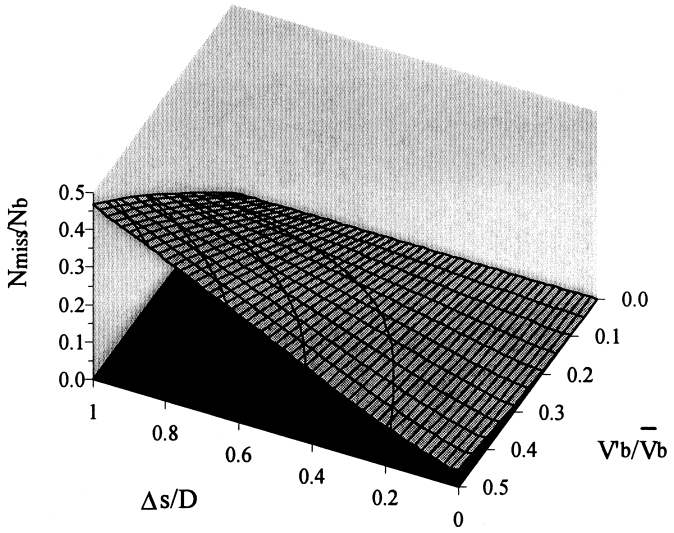

Fig. 4. Missing bubble fraction versus $\Delta s/D$ and $V'_b/\bar{V}_b$.

The harmonic mean of the measured velocity:

$$\overline{\left(\frac{1}{V_m}\right)}_{\text{normal}} = \frac{1}{\bar{V}_b} \frac{\int_0^{2\pi}\int_0^{\pi}\int_0^{\frac{\pi}{2}}\int_0^{2\pi} G \,\frac{\sin\xi \sin\mu\cos\mu}{4\pi^2}\,\mathrm{d}v\,\mathrm{d}\mu\,\mathrm{d}\xi\,\mathrm{d}\varphi}{\int_0^{2\pi}\int_0^{\pi}\int_0^{\frac{\pi}{2}}\int_0^{2\pi} \psi \,\frac{\sin\xi \sin\mu\cos\mu}{4\pi^2}\,\mathrm{d}v\,\mathrm{d}\mu\,\mathrm{d}\xi\,\mathrm{d}\varphi}, \tag{23}$$

where,

$$G = \begin{cases} \bar{V}_b/V_m & V_m \geq 0 \\ 0, & V_m < 0 \text{ or } \Delta < 0, \end{cases} \tag{24}$$

$$\psi = \begin{cases} 1, & V_m \geq 0 \\ 0, & V_m < 0 \text{ or } \Delta < 0, \end{cases} \tag{25}$$

$$V_m = V_i \left\{ \frac{[2(1 + H\mathbf{k}\cdot\mathbf{n}'_V) + \gamma((\mathbf{k} + H\mathbf{n}'_V)\cdot\mathbf{A}\cdot\mathbf{n}'_i)] + \sqrt{\Delta}}{2[\gamma(\mathbf{k}\cdot\mathbf{A}\cdot\mathbf{n}'_i) + 1]} \right\}, \tag{26}$$

$$\Delta = [2(1 + H\mathbf{k}\cdot\mathbf{n}'_V) + \gamma((\mathbf{k} + H\mathbf{n}'_V)\cdot\mathbf{A}\cdot\mathbf{n}'_i)]^2 - 4[\gamma(\mathbf{k}\cdot\mathbf{A}\cdot\mathbf{n}'_i) + 1]. \tag{27}$$

The harmonic mean of interfacial velocity in the surface normal direction for the normal case:

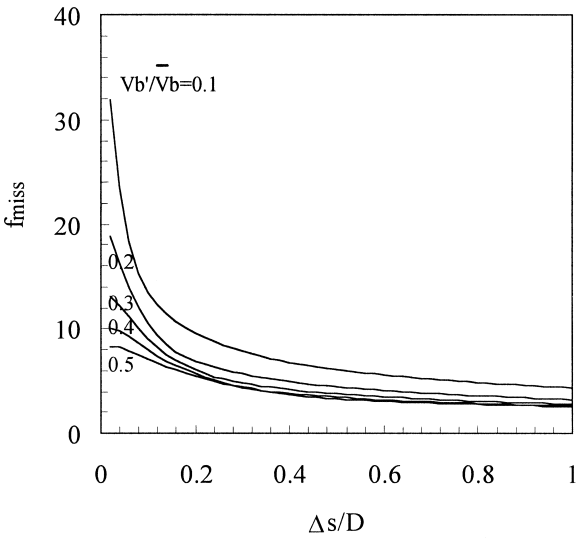

Fig. 5. f_{miss} versus $\Delta s/D$ and $V'_{\text{b}}/\bar{V}_{\text{b}}$.

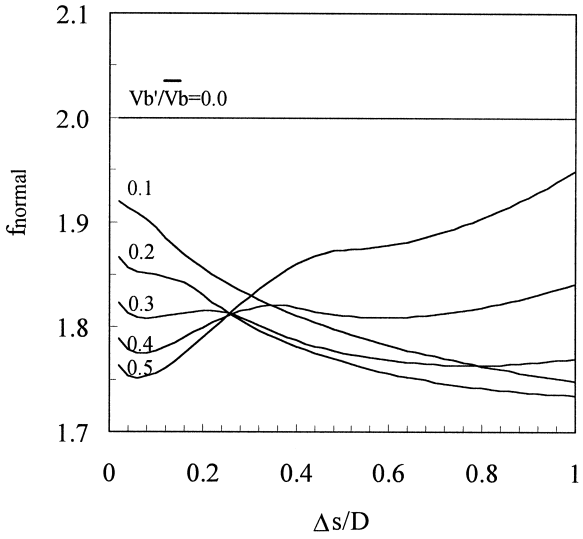

Fig. 6. f_{normal} versus $\Delta s/D$ and $V'_{\text{b}}/\bar{V}_{\text{b}}$.

$$\overline{\left(\frac{1}{V_i(\mathbf{n}_{\text{V}}\cdot\mathbf{n}_i)}\right)}_{\text{normal}} = \frac{1}{\bar{V}_{\text{b}}}\frac{\int_0^{2\pi}\int_0^{\pi}\int_0^{\frac{\pi}{2}}\int_0^{2\pi} Q_{\text{normal}}\dfrac{\sin\xi\sin\mu\cos\mu}{4\pi^2}\,\mathrm{d}v\,\mathrm{d}\mu\,\mathrm{d}\xi\,\mathrm{d}\varphi}{\int_0^{2\pi}\int_0^{\pi}\int_0^{\frac{\pi}{2}}\int_0^{2\pi}\psi\dfrac{\sin\xi\sin\mu\cos\mu}{4\pi^2}\,\mathrm{d}v\,\mathrm{d}\mu\,\mathrm{d}\xi\,\mathrm{d}\varphi}, \tag{28}$$

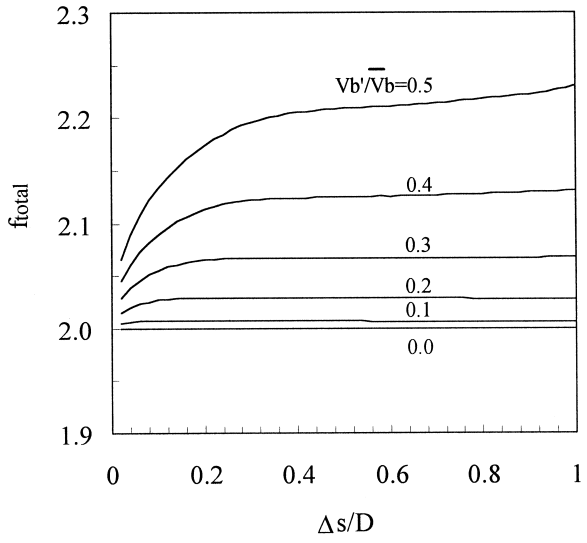

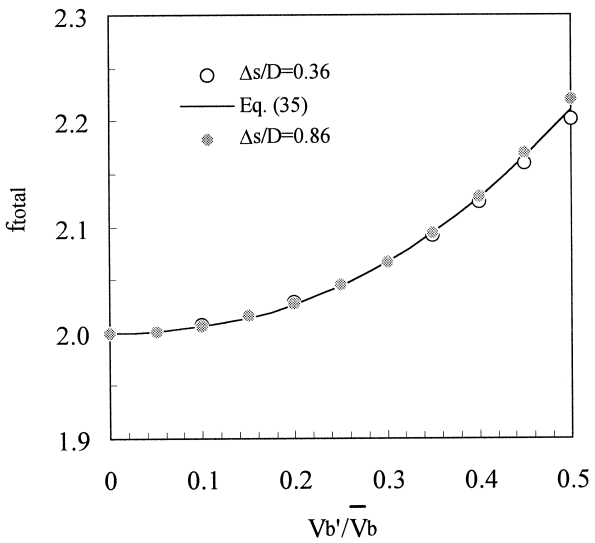

Fig. 7. (a) f_{total} versus $\Delta s/D$ and $V'_{\text{b}}/\bar{V}_{\text{b}}$. (b) f_{total} versus $V'_{\text{b}}/\bar{V}_{\text{b}}$ with $\Delta s/D$ between 0.36 and 0.86.

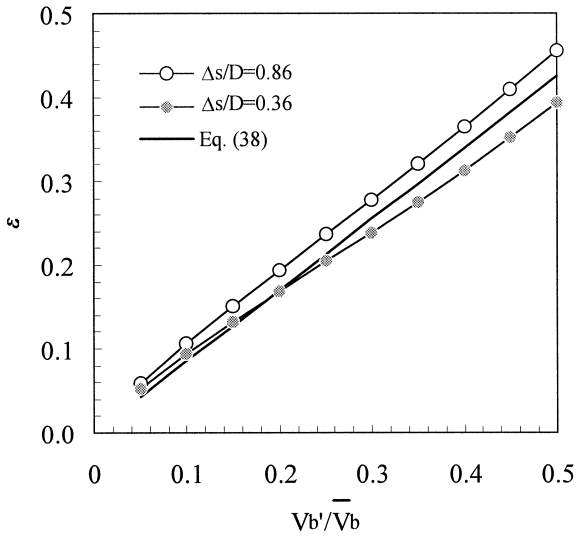

Fig. 8. Relation between $V'_b/\bar{V}_b$ and ϵ, the standard deviation of $1/V_m$.

where

$$Q_{\text{normal}} = \begin{cases} [(\mathbf{k} + H\mathbf{n}'_V) \cdot \mathbf{A} \cdot \mathbf{n}'_i]^{-1} & V_m \geq 0 \\ 0, & V_m < 0 \text{ or } \Delta < 0. \end{cases}, \tag{29}$$

The harmonic mean of interfacial velocity in the surface normal direction for missing bubbles:

$$\overline{\left(\frac{1}{V_i(\mathbf{n}_V \cdot \mathbf{n}_i)}\right)}_{\text{miss}} = \frac{1}{\bar{V}_b} \frac{\int_0^{2\pi}\int_0^{\pi}\int_0^{\frac{\pi}{2}}\int_0^{2\pi} Q_{\text{miss}} \frac{\sin\xi \sin\mu \cos\mu}{4\pi^2} \mathrm{d}v \, \mathrm{d}\mu \, \mathrm{d}\xi \, \mathrm{d}\varphi}{\int_0^{2\pi}\int_0^{\pi}\int_0^{\frac{\pi}{2}}\int_0^{2\pi} (1-\psi) \frac{\sin\xi \sin\mu \cos\mu}{4\pi^2} \mathrm{d}v \, \mathrm{d}\mu \, \mathrm{d}\xi \, \mathrm{d}\varphi}, \tag{30}$$

where

$$Q_{\text{miss}} = \begin{cases} [(\mathbf{k} + H\mathbf{n}'_V) \cdot \mathbf{A} \cdot \mathbf{n}'_i]^{-1}, & V_m < 0 \text{ or } \Delta < 0 \\ 0, & V_m \geq 0 \end{cases}. \tag{31}$$

It is difficult to analytically perform the integrations given in (22), (23), (28) and (30), particulaly for the explicit specification of the integration domain for the missing bubble cases. Hence, numerical investigation is inevitable. From the numerical solutions, the theoretical calibration factors, f_{total}, f_{normal} and f_{miss} can be obtained as functions of H and $\Delta s/D$. Based on (6), these theoretical calibration factors should also satisfy:

$$f_{\text{total}} = \left(\frac{N_{\text{b}} - N_{\text{miss}}}{N_{\text{b}}}\right) f_{\text{normal}} + \left(\frac{N_{\text{miss}}}{N_{\text{b}}}\right) f_{\text{miss}}. \tag{32}$$

The missed bubble number fraction is given by:

$$\left(\frac{N_{\text{miss}}}{N_{\text{b}}}\right) = \int_0^{2\pi}\int_0^{\pi}\int_0^{\frac{\pi}{2}}\int_0^{2\pi}(1-\psi)\frac{\sin\xi\sin\mu\cos\mu}{4\pi^2}\,\mathrm{d}v\,\mathrm{d}\mu\,\mathrm{d}\xi\,\mathrm{d}\varphi. \tag{33}$$

3. Results and discussions

The numerical integrations are conducted with ξ, φ, μ and v as the independent variables over the specified ranges. The results are summarized in Figs. 4–8, including the variations of the missed bubble number fraction, f_{total}, f_{normal} and f_{missing} with respect to different relative bubble velocity fluctuations and probe tip separations.

In Fig. 4, the missed bubble fraction grows monotonously as $\Delta s/D$ and $V'_{\text{b}}/\bar{V}_{\text{b}}$ increase. If the probe tip separation equals the measured bubble diameter with $V'_{\text{b}}/\bar{V}_{\text{b}}$ equal to 0.5, the missing bubble fraction reaches about 0.5. In other words, roughly 50% of the bubbles that pass through the first probe tip cannot give normal signals for the measurement of the local interfacial area concentration. Even when the probe tip separation reduces to zero, a certain number of bubbles are still missed if the bubble velocity has lateral components, because the probe tip order is still in effect, resulting missing bubble cases as identified in Fig. 2(c).

For the missed bubbles, the theoretical calibration factor, f_{miss}, is shown in Fig. 5 against the relative probe tip separation. As expected, when both $\Delta s/D$ and $V'_{\text{b}}/\bar{V}_{\text{b}}$ are relatively small, f_{miss} is very large. It implies that the harmonic mean of the missed interface velocities in the surface normal direction is much larger than the mean value of $\Delta t/\Delta s$. This is because the missed points are close to the region where the angle between the velocity direction and the surface normal is close to $\pi/2$. As $\Delta s/D$ and $V'_{\text{b}}/\bar{V}_{\text{b}}$ become very large, the missed number fraction increases, but the harmonic mean of the missed interface velocities in the surface normal direction is closer to the overall average value. Hence, f_{miss} drops significantly. In experiments, the conventional way to recover the interfacial area concentration carried by the missed bubbles at the measuring point, is to treat them as if they possess the average interface velocity in the surface normal direction for the normal case. The variation of f_{miss} suggests that this method is improper, due to the tremendous difference between the two values, particularly when the missing bubble fraction is small.

For the bubbles that give normal signals as demonstrated in Fig. 2(a), the theoretical calibration factor presents irregular responses to the variations of $\Delta s/D$ and $V'_{\text{b}}/\bar{V}_{\text{b}}$ as shown in Fig. 6. If the velocity fluctuation is zero, f_{normal} equals 2, which resembles the simplified case without missing bubbles as discussed in Section 2. The harmonic mean of the bubble interface normal velocity is twice the average of $\Delta t/\Delta s$. However, when the bubble velocity fluctuation increases slightly, $V'_{\text{b}}/\bar{V}_{\text{b}}$ equals 0.1 for instance, Fig. 6 shows the theoretical calibration factor becomes smaller than 2, and decreases monotonously as $\Delta s/D$ increases within the studied

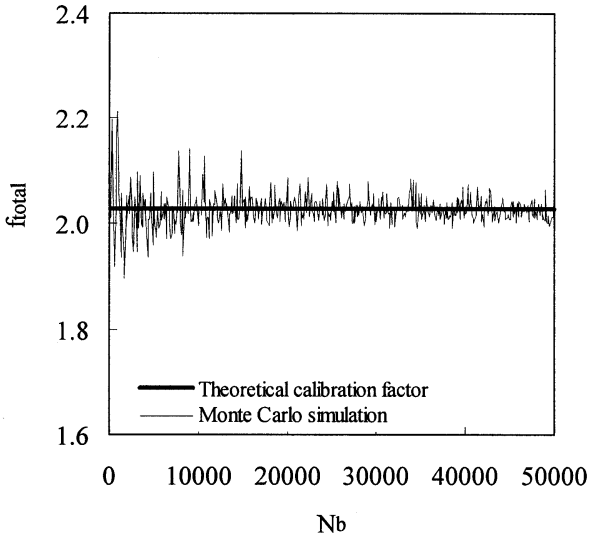

Fig. 9. f_{total} versus bubble number ($V'_{\text{b}}/\bar{V}_{\text{b}} = 0.2$ and $\Delta s/D = 0.5$).

range. The reason could have two folds. On the one hand, the harmonic mean of the bubble velocity in the surface normal direction losses some large components carried by the missed bubbles, resulting in smaller numerator in the expression of f_{normal}. On the other hand, the components of $\Delta t/\Delta s$ also becomes smaller, due to the possible situations when the two probe tips can poke the bubble surface almost simultaneously, if the probe-tip separation is smaller than the bubble diameter. The resultant denominator in the expression of f_{normal} decreases. Combining these two factors together, when the velocity fluctuation is small, the numerator drops faster than the denominator does as the probe-tip separation increases. Accordingly, f_{normal} shows a general decreasing trend. For larger bubble velocity fluctuation, $V'_{\text{b}}/\bar{V}_{\text{b}}$ equals 0.5, for instance, the mechanism becomes the opposite, and f_{normal} gradually increases as shown in Fig. 6, though bonded by the value of 2. In practical applications, such a complicated variation of f_{normal} has little help in calibrating the double-sensor conductivity probe. Even if it has to be done in this way, the information of f_{miss} and the missing bubble fraction should be incorporated into the process, as presented in (32), which would complicate the calibration procedure.

In spite of all the complexities in f_{normal} and f_{miss}, the overall theoretical calibration factor, f_{total}, demonstrates some valuable characteristics for the practical calibration of a double-sensor conductivity probe. As shown in Fig. 7(a), for fixed bubble velocity fluctuation, f_{total} is almost constant in the range of $\Delta s/D$ between 0.36 and 0.86. In other words, for fixed probe tip separation and bubble velocity fluctuation, the overall theoretical calibration factor keeps constant with bubble size ranging from about $1.2\Delta s$ to $3\Delta s$. This is rather important in most of the experiments where bubbles have size distributions. By plotting f_{total} against bubble velocity fluctuations, the two curves for $\Delta s/D$ equal to 0.36 and 0.86, respectively, collapse to a single line, and the relative difference is within 1.5%, Fig. 7(b). Fitting the curves gives the following formula for the overall theoretical calibration factor:

$$f_{\text{total}} = 2 + \left(\frac{V'_{\text{b}}}{\bar{V}_{\text{b}}}\right)^{2.25}, \quad D = 1.2\Delta s \sim 3\Delta s. \tag{34}$$

Consequently, the local interfacial area concentration is given by:

$$\bar{a}_i^{\text{t}} = \left(\frac{2N_{\text{b}}}{\Delta s \Delta T}\right)\left[2 + \left(\frac{V'_{\text{b}}}{\bar{V}_{\text{b}}}\right)^{2.25}\right]\left[\frac{\sum_j(\Delta t_j)}{N_{\text{b}} - N_{\text{miss}}}\right], \quad D = 1.2\Delta s \sim 3\Delta s. \tag{35}$$

Within the specified bubble size range, this formula is valid regardless how many bubbles are missed in the measurement, as long as the output signals of the probe are proper for bubble identification, and the sample size is sufficiently large. Moreover, it gives flexibility to the probe spacing design. For a given mean size of the bubbles to be measured, the probe-tip separation can be chosen around half of the mean bubble diameter. If the bubbles are assumed to be spherical and the sample size is large enough, for bubble size varying from roughly 0.6–1.4 $\overline{D}$, the interfacial area concentration computed from (35) should be quite accurate, with a relative error less than $\pm 1.5\%$.

The remaining question is how to determine the relative bubble velocity fluctuation, namely $V'_{\text{b}}/\bar{V}_{\text{b}}$. One way is to build a relationship between the bubble velocity fluctuation and the relative standard deviation of the measured velocity, V_{m}, similar to the approach of Kataoka et al. (1986). However, because the measured velocity may have very large values when the two probe tips hit the bubble surface almost simultaneously with a very short time delay, the standard deviation of the measured velocity can be very high and inaccurate, as long as the finite samples do contain such values in the measurement. To overcome this shortcoming, the relative standard deviation of the inverse of the measured velocity is suggested here to characterize the bubble velocity fluctuation. This relative standard deviation, ϵ, is defined as:

$$\epsilon = \frac{\sigma_1/v_m}{(1/V_{\text{m}})} = \frac{\sqrt{\overline{(1/V_{\text{m}} - \overline{(1/V_{\text{m}})})^2}}}{\overline{(1/V_{\text{m}})}} = \frac{\sqrt{N_{\text{b}}\sum_j(\Delta t_j)^2 - (\sum_j \Delta t_j)^2}}{\sum_j \Delta t_j}, \tag{36}$$

where all the averaging operations are performed in the normal measurement case with the subscript "normal" dropped for simplicity. Similar to the harmonic mean of the measured velocity, this relative standard deviation can be related to the relative bubble velocity fluctuation. For the probe-tip separations of $0.36D$ and $0.86D$, the numerical solutions of ϵ, the relative standard deviation of $1/V_{\text{m}}$, versus $V'_{\text{b}}/\bar{V}_{\text{b}}$ is shown in Fig. 8, which satisfies the following linear function with an error of $\pm 10\%$.

$$\epsilon = \frac{\sigma_1/V_{\text{m}}}{\overline{(1/V_{\text{m}})}} \approx 0.85\left(\frac{V'_{\text{b}}}{V_{\text{b}}}\right), \quad D = 1.2\Delta s \sim 3\Delta s. \tag{37}$$

This error would cause $\pm 2\%$ fluctuations in the theoretical total calibration factor, f_{total}. It should be mentioned that in the investigated ranges, the maximum modification due to the existence of the bubble lateral movements, is only about 10% higher than 2, a factor without considering the effects of the bubble velocity fluctuation. According to Serizawa et al. (1975), the bubble velocity fluctuation is usually less than 0.4, and, therefore, the modification is even smaller, less than 7%. This correction may be overwhelmed by the statistic fluctuations of the

two-phase flow. Even if the two-phase flow is stable, the finite sample size in any experiment would induce considerable fluctuations to the measured parameter. To evaluate the proper sample size, a Monte Carlo scheme is developed using (22) and (23) to generate $(1/V_i)$ and $(1/V_m)$ with random angles of relevant probability distributions. The resultant total calibration factor for $V'_b/\bar{V}_b = 0.2$ and $\Delta s/D = 0.5$, is presented in Fig. 9 against the sample size. As the bubble number increases from 100 to 50,000, the statistic fluctuation of f_{total} decreases gradually from about $\pm 10\%$ to $\pm 1.5\%$. Usually, for a bubbly flow of 10% void fraction with bubble sizes of 2–4 mm in diameter and a liquid superficial velocity of about 1 m/s, 10,000 bubble samples would spend roughly 5 min, without taking account of the data processing process. It is thus very time-consuming to reduce the inherent statistic fluctuation. For practical applications, at least several thousands of bubbles need to be sampled, which would result in a statistical error of $\pm 7\%$, about the same magnitude of the maximum modification from the bubble velocity fluctuations.

Other factors, such as the near-spherical bubble shape and the possible bubble–probe interactions, may also contribute to the measurement error. Therefore, it would be fair to conclude that the effects of the bubble velocity fluctuation and the probe-tip separation are insignificant if the probe spacing is chosen roughly half of the mean diameter of the bubbles to be measured. Nevertheless, the bubble velocity fluctuation causes a systematic shift of the total calibration factor by (34). This investigation rigorously answered the question concerning the influences of the bubble lateral movement and the probe-tip separation.

4. Conclusions

Sensitivity studies on the measurement of the local time-averaged interfacial area concentration using a double-sensor conductivity probe, was carried out by considering the influences of the bubble lateral motion and the probe spacing. The basic assumptions in the analysis are isotropic bubble velocity fluctuations and spherical bubble shapes. Taking into account the influences of the bubble lateral movements and the finite probe spacing, the measurement mechanisms were closely examined to explain the missing bubble phenomena that occurred in data processing. Accordingly, three theoretical calibration factors were proposed to bridge the mean measurable parameter to the local interfacial area concentrations carried by the measured bubbles, the missed bubbles and their combination. To obtain these factors, the measurable value, $\Delta s/\Delta t$, was rigorously related to the bubble velocity in the surface normal direction, and the probability density function of each individual variable was identified with a proper coordinate transform. Numerical solutions of these theoretical calibration factors indicate that only the total calibration factor has practical value for applications. With the probe spacing ranging from 36 to 86% of the mean bubble diameter, the probe spacing has little effect on the total calibration factor. An approximate formula for this factor was provided with the relative bubble velocity fluctuation as the independent variable. Different from the result of Kataoka et al. (1986), the resultant local interfacial area concentration is greater than that without considering the lateral bubble velocity components. However, the modification is less than 7% for the reported maximum bubble velocity fluctuation in dispersed air–water bubbly flow if the probe spacing is within the specified range. To determine the

bubble velocity fluctuation in terms of the measured values, an appropriate method was also provided to avoid possible singularity problems due to the finite sample base. Moreover, for reasonable statistic behaviors in measurements, the necessary sample size was suggested using a Monte Carlo approach. Some other parameters, such as missing bubble number fraction and the interfacial area concentration carried by the missed bubbles, were also included for better understandings of the measurement mechanisms of a double-sensor conductivity probe. Detailed analyses about the missing bubble cases suggest that the missed bubbles contribute larger interfacial area concentration to the measuring point than the average value from the measured bubbles. Hence, the conventional concept for the recovery of the missed bubbles may cause uncertainty.

The present study assumes isotropic bubble velocity fluctuations and spherical bubble shapes. For some other practical bubble velocity distributions, however, the proposed method in this study is still valid by simply replacing the distribution function. On the other hand, the hypothesis on the bubble sphericity greatly simplifies the analysis, and further studies are needed for the measurement of non-spherical bubbles. For distorted or cap bubbles, the bubble-probe interactions, as well as the unpredictable surface normal directions, make the measurement virtually impossible. In such a situation, a four-sensor probe technique was proposed to depict the actual velocity direction of an interface (Kataoka et al. 1986). Moreover, the experimental evaluations of the proposed theoretical calibration factor should be performed by means of other measurement techniques, in order to estimate the possible influences of the basic assumptions.

Acknowledgement

This work was performed under the auspices of the U. S. Department of Energy.

Appendix A

At the moment, when the first probe tip hits a spherical bubble of diameter D, a rectangular coordinate system is chosen with its origin at the center of the bubble and its z-axis parallel to the probe orientation. In this coordinate system, the position on the bubble surface, where the first probe tip is located, can be expressed as a vector $\mathbf{r}$, which satisfies:

$$\mathbf{r} \cdot \mathbf{r} = \left(\frac{D}{2}\right)^2. \tag{A1}$$

After a time interval Δt, the bubble center moves to a position $\mathbf{V}_i \Delta t$ with a velocity $\mathbf{V}_i$, and the bubble surface hits the second probe tip at $(\mathbf{r} + \Delta s\ \mathbf{k})$, which also satisfies the equation of sphere:

$$(\mathbf{r}+\Delta s\mathbf{k}-\mathbf{V}_i\Delta t)\cdot(\mathbf{r}+\Delta s\mathbf{k}-\mathbf{V}_i\Delta t)=\left(\frac{D}{2}\right)^2. \tag{A2}$$

Subtracting (A1) from (A2) and dividing the resultant equation with Δt, we have:

$$\left[\left(\frac{\Delta s}{\Delta t}\right)\mathbf{k}-V_i\mathbf{n}_V\right]\cdot\left[\left(\frac{D}{\Delta s}\right)\left(\frac{\Delta s}{\Delta t}\right)\mathbf{n}_i+\left(\frac{\Delta s}{\Delta t}\right)\mathbf{k}-V_i\mathbf{n}_V\right]=0, \tag{A3}$$

where $\mathbf{n}_V$ is the unit vector of the bubble velocity and $\mathbf{n}_i$ is the surface normal vector (unit vector of $\mathbf{r}$). This equation can be further simplified as:

$$\eta^2(\gamma\mathbf{k}\cdot\mathbf{n}_i+1)-\eta[2(\mathbf{k}\cdot\mathbf{n}_V)+\gamma(\mathbf{n}\cdot\mathbf{n}_V)]+1=0, \tag{A4}$$

with:

$$V_m=\left(\frac{\Delta s}{\Delta t}\right),\ \eta=\left(\frac{V_m}{V_i}\right)\quad\text{and}\quad\gamma=\left(\frac{D}{\Delta s}\right). \tag{A5}$$

Accordingly, η, the ratio between the measurable "velocity" and the bubble velocity, can be obtained by solving (A4):

$$\eta=\frac{V_m}{V_i}=\frac{2(\mathbf{k}\cdot\mathbf{n}_V)+\gamma(\mathbf{n}_i\cdot\mathbf{n}_V)]+\sqrt{[2(\mathbf{k}\cdot\mathbf{n}_V)+\gamma(\mathbf{n}_i\cdot\mathbf{n}_V)]^2-4[\gamma(\mathbf{k}\cdot\mathbf{n}_i)+1]}}{2[\gamma(\mathbf{k}\cdot\mathbf{n}_i)+1]}. \tag{A6}$$

Here, one root of η is dropped, because it refers to the solution for the second probe tip to hit the surface from the inside of the bubble. This equation gives the general relation between the bubble velocity and the measurable velocity. When the bubble velocity fluctuation is negligible, the velocity direction of each individual bubble follows the bulk liquid flow. With the probe aligned to the flow direction, (A6) can be simplified to:

$$\eta=\frac{V_m}{V_i}=1. \tag{A7}$$

This is exactly the ideal case we discussed in Section 2, with the measured velocity identical to the bubble speed.

When the probe tip separation is small in comparison with the bubble diameter, $\Delta s\ll D$, (A6) can be readily reduced to:

$$\eta=\frac{V_m}{V_i}=\frac{\mathbf{n}_V\cdot\mathbf{n}_i}{\mathbf{k}\cdot\mathbf{n}_i}. \tag{A8}$$

This is exactly the same as the solution of Kataoka et al. (1986).

References

Boure, J.A., 1978. Mathematical modeling of two-phase flows. In: S. Banerjee, K.R. Weaver (Ed.). In: Proceedings of CSNI Specialist Meeting, Vol. 1. A.E.C.L., Toronto, p. 85.

Herringe, R.A., Davis, M.R., 1976. Structural development of gas-liquid mixture flow. J. Fluid Mech. 73, 97–123.

Ishii, M., 1975. Thermo-Fluid Dynamic Theory of Two-Phase Flow. Collection de la Direction des Etudes et Reserches d'Electricité de France, Eyrolles, Paris.

Kataoka, I., Ishii, M., Serizawa, A., 1986. Local formulation and measurements of interfacial area concentration in two-phase flow. Int. J. Multiphase Flow 12 (4), 505.

Kataoka, I., Ishii, M., Serizawa, A., 1994. Sensitivity analysis of bubble size and probe geometry on the measurements of interfacial area concentration in gas-liquid two-phase flow. J. Nucl. Engng. & Design 146, 53–70.

Landau, J., 1977. Comparison of methods of measuring interfacial areas in gas–liquid dispersions. Canadian J. Chem. Engng. 55, 13.

Leung, W.H., 1996. Modeling of interfacial area concentration and interfacial momentum transfer: Theoretical and experimental study. Ph. D. Thesis. Dept. of Nuclear Engineering, Purdue University, West Lafayette, IN, USA.

Serizawa, A., Kataoka, I., Michiyoshi, I., 1975. Turbulent structure of air-water bubbly flow II. Local properties. Int. J. Multiphase Flow 2, 235–246.

Vernier, P., Delhaye, J.M., 1968. General two-phase flow equations applied to the thermohydrodynamics of boiling nuclear reactor. Engng. Primaire 1, 5.

Veteau, J.M., Charlot, R., 1981. Interfacial area concentration measurements in two-phase bubbly flow: comparison between the light attenuation technique and a local method. European Two-phase Flow Group Meeting, Eindhoven, (The Netherlands), June 2–5.